

$z \rightarrow -z$ Symmetry of Spin-Orbit Coupling and Weak Localization in Graphene

Edward McCann and Vladimir I. Fal'ko

Department of Physics, Lancaster University, Lancaster, LA1 4YB, United Kingdom

(Received 22 November 2011; published 20 April 2012)

We show that the influence of spin-orbit (SO) coupling on the weak-localization effect for electrons in graphene depends on the lack or presence of $z \rightarrow -z$ symmetry in the system. While, for $z \rightarrow -z$ asymmetric SO coupling, disordered graphene should display a weak antilocalization behavior at lowest temperature, $z \rightarrow -z$ symmetric coupling leads to an effective saturation of decoherence time which can be partially lifted by an in-plane magnetic field, thus tending to restore the weak-localization effect.

DOI: 10.1103/PhysRevLett.108.166606

PACS numbers: 72.80.Vp, 71.70.Ej, 73.20.Fz, 81.05.ue

The effect of spin-orbit (SO) coupling in graphene represents an example of a stimulating theoretical study that remains difficult to detect experimentally. The form of intrinsic SO coupling in the graphene band structure, suggested by Kane and Mele [1], has fueled the theory of Z_2 topological insulators, but its strength is too weak for detection by conventional spectroscopic methods [1–5]. Here, we show how the presence of SO coupling in disordered graphene could be manifested in quantum transport measurements. Specifically for graphene, the presence of SO coupling may not necessarily lead to antilocalization behavior known in semiconductors and metals [6], and this reflects the presence or lack of $z \rightarrow -z$ symmetry in the source or microscopic origin of SO coupling.

In general, weak localization is very sensitive to symmetry breaking in the electronic system or to scattering involving electron spin, since it is formed by electrons propagating along long diffusive trajectories [6–16]. The typical behavior of electrons in metals with strong SO coupling results in a pronounced weak antilocalization effect manifested by positive magnetoresistance, in contrast to simple metals and semiconductors where the weak-localization magnetoresistance caused by the interference correction to conductivity is negative. In metallic graphene, if the influence of SO coupling may be neglected, then the presence of intervalley scattering results in conventional weak localization [8–15]. Then, at the lowest temperatures, we find that SO interaction leads to weak antilocalization, as in the typical case, but only if graphene has broken $z \rightarrow -z$ symmetry, due to a substrate or deposits. In contrast, for a $z \rightarrow -z$ symmetric system, SO coupling leads only to a saturation in the size of the weak-localization correction rather than antilocalization, which can be taken for a saturation of $\tau_\varphi(T)$ as $T \rightarrow 0$. We analyze the influence of an in-plane magnetic field on the interference correction to conductivity for both $z \rightarrow -z$ symmetric and antisymmetric SO-coupling scenarios and find that it lifts the aforementioned saturation of τ_φ . Note that a $z \rightarrow -z$ symmetric SO-coupling term in graphene may be promoted even by sp^3 hybridization of asymmetrically deposited impurities [17].

The breaking of $z \rightarrow -z$ symmetry in pristine graphene is usually associated with the addition of a Bychkov-Rashba term \hat{h}_{BR} [1–3,5,16–19] to the intrinsic SO coupling \hat{h}_{KM} [1,3,4,16] in the graphene Hamiltonian:

$$\hat{H} = v\mathbf{\Sigma}\mathbf{p} + \hat{h}_{\text{KM}} + \hat{h}_{\text{BR}} + \hat{U} + \hat{V}_{\text{sym}} + \hat{V}_{\text{asy}} + \mu_B\mathbf{s}\mathbf{B}_{\parallel},$$

$$\hat{h}_{\text{KM}} = \lambda\Sigma_z s_z, \quad \hat{h}_{\text{BR}} = \mu(\Sigma_x s_y - \Sigma_y s_x). \quad (1)$$

The last term in \hat{H} accounts for Zeeman splitting due to the in-plane magnetic field $\mathbf{B}_{\parallel} = \hat{\ell}B_{\parallel}$, and the terms

$$\hat{U} = u_0\hat{I} + \sum_{a,l=x,y,z} u_{a,l}\Sigma_a\Lambda_l, \quad (2)$$

$$\hat{V}_{\text{sym}} = s_z \left[\sum_{a=x,y,z} \alpha_{a,z}\Sigma_a + \sum_{l=x,y,z} \beta_{l,z}\Lambda_l \right], \quad (3)$$

$$\hat{V}_{\text{asy}} = \sum_{j=x,y} s_j \left[\sum_{a=x,y,z} \alpha_{a,j}\Sigma_a + \sum_{l=x,y,z} \beta_{l,j}\Lambda_l \right] \quad (4)$$

describe three types of disorder on the honeycomb lattice: spin-independent perturbations, SO coupling with $z \rightarrow -z$ symmetric perturbations, and $z \rightarrow -z$ asymmetric perturbations, respectively. Here, we use a symmetry-based approach to determine how electronic spin may be combined with lattice and valley degrees of freedom. We focus on the region near the Fermi level which lies in the vicinity of two inequivalent corners of the Brillouin zone, known as valleys, with wave vectors $\mathbf{K}_{\pm} = \pm(4\pi/3a, 0)$, where a is the lattice constant, and the momentum measured from the center of a valley is $\mathbf{p} = \hbar\mathbf{k} - \hbar\mathbf{K}_{\pm}$. The Hamiltonian (1) operates in a space of eight-component Bloch functions $\Phi = [\phi_{\mathbf{K}_{+A}\uparrow}, \phi_{\mathbf{K}_{+B}\uparrow}, \phi_{\mathbf{K}_{-B}\uparrow}, \phi_{\mathbf{K}_{-A}\uparrow}, \phi_{\mathbf{K}_{+A}\downarrow}, \phi_{\mathbf{K}_{+B}\downarrow}, \phi_{\mathbf{K}_{-B}\downarrow}, \phi_{\mathbf{K}_{-A}\downarrow}]$ consisting of two valleys $\mathbf{K}_{+}/\mathbf{K}_{-}$, two lattice sites A/B , and two spin components \uparrow/\downarrow . We use three sets of Pauli matrices [11,12] to describe spin $\vec{s} = (s_x, s_y, s_z)$, sublattice “isospin” $\vec{\Sigma} = (\Sigma_x, \Sigma_y, \Sigma_z)$, and valley “pseudospin” $\vec{\Lambda} = (\Lambda_x, \Lambda_y, \Lambda_z)$ [20]. The matrices \vec{s} , $\vec{\Sigma}$, and $\vec{\Lambda}$ all change sign upon time inversion so that their products are time-inversion symmetric, and $\Sigma_a s_j$ and $s_j \Lambda_l$

may be used as a basis for a phenomenological description of static disorder leading to SO scattering.

The results of this symmetry-based approach are summarized in Table I, which shows how \vec{s} , $\vec{\Sigma}$, and $\vec{\Lambda}$ may be combined to form irreducible representations of the planar group C'_{6v} [21], which combines the point group C_{6v} of strictly two-dimensional graphene with primitive translations, as appropriate for the description of two valleys \mathbf{K}_{\pm} . Matrices $\vec{\Sigma}$ and $\vec{\Lambda}$ are confined to the two-dimensional plane of graphene, and their behavior under symmetry operations is impervious to the third spatial dimension. Thus, they are invariant under mirror reflection in the graphene plane so that, in the absence of spin, they only appear in the representations that are $z \rightarrow -z$ symmetric. The presence of spin, however, introduces a pseudovector that lies in three-dimensional space: s_z is even under $z \rightarrow -z$ reflection, but in-plane components s_x and s_y are odd. Thus, SO terms containing s_z appear in $z \rightarrow -z$ symmetric representations, and terms containing s_x and s_y appear in $z \rightarrow -z$ asymmetric representations.

In Table I, $\Sigma_z s_z$ is an invariant of the point group of graphene representing intrinsic Kane-Mele SO coupling \hat{h}_{KM} [1,3,4,16] and $\Sigma_x s_y - \Sigma_y s_x$ describes the Bychkov-Rashba term \hat{h}_{BR} [1–3,5,16–19], which assumes the existence of a transverse field $\vec{\ell}_z$ breaking $z \rightarrow -z$ symmetry. The entries in Table I take into account possible SO scattering mechanisms due to defects in graphene: \hat{V}_{sym} includes terms proportional to s_z , and \hat{V}_{asy} includes s_x and

s_y . The term \hat{U} , Eq. (2), describes disorder decoupled from the spin degree of freedom: $u_0(\mathbf{r})\hat{I}$ describing the influence of remote charges, $u_{z,z}(\mathbf{r})\Sigma_z\Lambda_z$ describing different on-site energies of the A/B sublattices, and $u_{x,z}(\mathbf{r})\Sigma_x\Lambda_z$ and $u_{y,z}(\mathbf{r})\Sigma_y\Lambda_z$ accounting for fluctuations of A/B hopping. The other terms in \hat{U} , $u_{a,x}(\mathbf{r})\Sigma_a\Lambda_x$ and $u_{a,y}(\mathbf{r})\Sigma_a\Lambda_y$ for $a = x, y, z$, generate intervalley scattering. We assume that different types of disorder in the Hamiltonian are uncorrelated and x - y isotropic:

$$\langle u_{a,l}(\mathbf{r})u_{a',l'}(\mathbf{r}') \rangle = u_{a,l}^2 \delta_{aa'} \delta_{ll'} \delta(\mathbf{r} - \mathbf{r}'),$$

$$\langle \alpha_{a,j}(\mathbf{r})\alpha_{a',j'}(\mathbf{r}') \rangle = \alpha_{a,j}^2 \delta_{aa'} \delta_{jj'} \delta(\mathbf{r} - \mathbf{r}'),$$

$$\langle \beta_{l,j}(\mathbf{r})\beta_{l',j'}(\mathbf{r}') \rangle = \beta_{l,j}^2 \delta_{ll'} \delta_{jj'} \delta(\mathbf{r} - \mathbf{r}').$$

In the following study, we employ the standard diagrammatic technique for disordered systems [6,7] to calculate the weak-localization correction $\delta\sigma$ to the conductivity in the metallic regime $p_F v \tau \gg \hbar$. We assume that the Dirac-like Hamiltonian $v\Sigma \cdot \mathbf{p}$ dominates the electronic behavior and that diagonal disorder, $\hat{I}u_0(\mathbf{r})$ in Eq. (2), determines the elastic scattering rate, $\tau^{-1} \approx \tau_0^{-1} = \pi\gamma u^2/\hbar$, where $\gamma = p_F/(2\pi\hbar^2 v)$ is the density of states per spin, per valley [11,12]. The current operator corresponding to the Dirac-like Hamiltonian is momentum-independent, so that the current vertex entering the Drude conductivity is renormalized by vertex corrections. Then, the Drude conductivity is equal to $\sigma = 4e^2\gamma D$, where the diffusion coefficient is $D = v^2\tau_{\text{tr}}/2$ and the transport time is twice the scattering time, $\tau_{\text{tr}} = 2\tau_0$ [8].

TABLE I. Irreducible representations of the planar group C'_{6v} [21], as provided by the matrices Σ_a , Λ_l , and s_j . Representations A_1 , A_2 , B_1 , B_2 , E_1 , and E_2 are part of the point group of two-dimensional graphene C_{6v} ; representations E'_1 , E'_2 , and G' incorporate primitive translations, and $z \rightarrow -z$ asymmetric representations are identified by an overscript, e.g., \tilde{A}_1 [22].

Irreducible representation	$z \rightarrow -z$ symmetric	$z \rightarrow -z$ asymmetric [22]
A_1 (\tilde{A}_1)	$\hat{I}, \Sigma_z s_z$	$\Sigma_x s_y - \Sigma_y s_x$
A_2 (\tilde{A}_2)	Σ_z, s_z	$\Sigma_x s_x + \Sigma_y s_y$
B_1 (\tilde{B}_1)	Λ_z	
B_2 (\tilde{B}_2)	$\Sigma_z \Lambda_z, \Lambda_z s_z$	
E_1 (\tilde{E}_1)	$\begin{pmatrix} \Sigma_x \\ \Sigma_y \end{pmatrix}, \begin{pmatrix} -\Sigma_y s_z \\ \Sigma_x s_z \end{pmatrix}$	$\begin{pmatrix} s_x \\ s_y \end{pmatrix}, \begin{pmatrix} -\Sigma_z s_y \\ \Sigma_z s_x \end{pmatrix}$
E_2 (\tilde{E}_2)	$\begin{pmatrix} \Lambda_z \Sigma_x \\ \Lambda_z \Sigma_y \end{pmatrix}$	$\begin{pmatrix} \Sigma_x s_y + \Sigma_y s_x \\ \Sigma_x s_x - \Sigma_y s_y \end{pmatrix}, \begin{pmatrix} -\Lambda_z s_y \\ \Lambda_z s_x \end{pmatrix}$
E'_1 (\tilde{E}'_1)	$\begin{pmatrix} \Lambda_x \Sigma_z \\ \Lambda_y \Sigma_z \end{pmatrix}, \begin{pmatrix} \Lambda_x s_z \\ \Lambda_y s_z \end{pmatrix}$	
E'_2 (\tilde{E}'_2)	$\begin{pmatrix} \Lambda_x \\ \Lambda_y \end{pmatrix}$	
G' (\tilde{G}')	$\begin{pmatrix} \Lambda_x \Sigma_y \\ -\Lambda_x \Sigma_x \\ \Lambda_y \Sigma_x \\ \Lambda_y \Sigma_y \end{pmatrix}$	$\begin{pmatrix} \Lambda_x s_x \\ \Lambda_x s_y \\ \Lambda_y s_x \\ \Lambda_y s_y \end{pmatrix}$

The weak-localization correction $\delta\sigma$ may be written in terms of disorder-averaged two-particle correlation functions known as Cooperon propagators C_j^l , where the index l refers to pseudospin (related to $\vec{\Lambda}$ describing valley degrees of freedom) and j refers to spin (related to \vec{s}). All the Cooperons that we consider are singlets with respect to sublattice isospin $\vec{\Sigma}$ because all isospin-triplet modes have relaxation gaps $\sim 1/\tau_0$ [11, 12]. Then, $\delta\sigma$ may be written in terms of a summation with respect to 16 Cooperons consisting of combinations of spin and pseudospin singlet and triplets:

$$\delta\sigma = \frac{e^2 D}{\pi\hbar} \sum_{j,l=0,x,y,z} c_j c_l C_j^l(\mathbf{r}' = \mathbf{r}),$$

$$\left[D \left(i\nabla + \frac{2e\mathbf{A}}{c\hbar} \right)^2 + \Gamma_j^l + \tau_\varphi^{-1} - i\omega \right] C_j^l(\mathbf{r}, \mathbf{r}') = \delta(\mathbf{r} - \mathbf{r}'). \quad (5)$$

Here, the factors $c_0 = 1$ and $c_x = c_y = c_z = -1$ take into account the fact that singlet and triplet Cooperons (of both spin and pseudospin) appear with opposite signs, and \mathbf{A} is the vector potential of the homogeneous external magnetic field, $\mathbf{B} = \text{rot}\mathbf{A}$ ($B_z = \partial_x A_y - \partial_y A_x$).

Inelastic dephasing is taken into account in Eq. (5) by τ_φ^{-1} , and, in general, symmetry-breaking perturbations [such as those contained in the Hamiltonian Eq. (1)] contribute relaxation gaps Γ_j^l to the otherwise gapless Cooperons C_j^l , as quantified in terms of relaxation rates summarized in Table II. Then, the zero-field temperature-dependent correction, $\delta\rho(0)$, to the sheet resistance, where $\delta\rho(0)/\rho^2 \equiv -\delta\sigma$, may be written as

$$\delta\rho(0) = -\frac{e^2 \rho^2 D}{\pi\hbar} \sum_{j,l=0,x,y,z} c_j c_l \int_0^{(D\tau)^{-1/2}} \frac{q dq}{2\pi} C_j^l(q), \quad (6)$$

$$= -\frac{e^2 \rho^2}{2\pi\hbar} \sum_{j,l=0,x,y,z} c_j c_l \ln \left(\frac{\tau^{-1}}{\tau_\varphi^{-1} + \Gamma_j^l} \right), \quad (7)$$

TABLE II. Scattering rates, due to symmetry-breaking terms in the Hamiltonian Eq. (1), that produce relaxation gaps Γ_j^l in the otherwise gapless Cooperons C_j^l where j refers to spin and l to valley. The relaxation rate of the intervalley Cooperons τ_*^{-1} and the intervalley rate τ_{iv}^{-1} result from spin-independent disorder; intrinsic τ_{KM}^{-1} and Bychkov-Rashba τ_{BR}^{-1} rates arise from the coupling of spin and lattice; and rates $\tau_{zv,e}^{-1}$, $\tau_{zv,o}^{-1}$, $\tau_{iv,e}^{-1}$, and $\tau_{iv,o}^{-1}$ account for the coupling of valley and spin degrees of freedom.

Relaxation gaps	Relaxation rates
$\Gamma_0^0 = 0$	$\tau_*^{-1} = \tau_z^{-1} + \tau_{iv}^{-1}$
$\Gamma_0^y = \Gamma_0^x = \tau_*^{-1} + 2\tau_{zv,e}^{-1} + 4\tau_{zv,o}^{-1} + 2\tau_{iv,e}^{-1} + 4\tau_{iv,o}^{-1}$	$\tau_{iv}^{-1} = \pi\gamma(u_{x,x}^2 + u_{x,y}^2 + u_{y,x}^2 + u_{y,y}^2 + u_{z,x}^2 + u_{z,y}^2)/\hbar$
$\Gamma_0^z = 2\tau_{iv}^{-1} + 4\tau_{iv,e}^{-1} + 8\tau_{iv,o}^{-1}$	$\tau_z^{-1} = 2\pi\gamma(u_{x,z}^2 + u_{y,z}^2 + u_{z,z}^2)/\hbar$
$\Gamma_x^0 = \Gamma_y^0 = \tau_{\text{BR}}^{-1} + \tau_{\text{KM}}^{-1} + 2\tau_{zv,e}^{-1} + 2\tau_{zv,o}^{-1} + 4\tau_{iv,e}^{-1} + 4\tau_{iv,o}^{-1}$	$\tau_{\text{KM}}^{-1} = \lambda^2/(\epsilon_F^2 \tau_0) + 2\pi\gamma(\alpha_{x,z}^2 + \alpha_{y,z}^2 + \alpha_{z,z}^2)/\hbar$
$\Gamma_x^x = \Gamma_x^y = \Gamma_y^x = \Gamma_y^y =$	$\tau_{\text{BR}}^{-1} = 2\tau_0 \mu^2/\hbar^2 + \pi\gamma(\alpha_{x,x}^2 + \alpha_{x,y}^2 + \alpha_{y,x}^2 + \alpha_{y,y}^2 + \alpha_{z,x}^2 + \alpha_{z,y}^2)/\hbar$
$\tau_*^{-1} + \tau_{\text{BR}}^{-1} + \tau_{\text{KM}}^{-1} + 2\tau_{zv,e}^{-1} + 2\tau_{iv,e}^{-1} + 4\tau_{iv,o}^{-1}$	$\tau_{zv,e}^{-1} = \pi\gamma\beta_{z,z}^2/\hbar$
$\Gamma_x^z = \Gamma_y^z = 2\tau_{iv}^{-1} + \tau_{\text{BR}}^{-1} + \tau_{\text{KM}}^{-1} + 2\tau_{zv,e}^{-1} + 2\tau_{zv,o}^{-1} + 4\tau_{iv,o}^{-1}$	$\tau_{iv,e}^{-1} = \pi\gamma\beta_{x,z}^2/\hbar = \pi\gamma\beta_{y,z}^2/\hbar$
$\Gamma_z^0 = 2\tau_{\text{BR}}^{-1} + 4\tau_{zv,o}^{-1} + 8\tau_{iv,o}^{-1}$	$\tau_{zv,o}^{-1} = \pi\gamma\beta_{z,x}^2/\hbar = \pi\gamma\beta_{z,y}^2/\hbar$
$\Gamma_z^x = \Gamma_z^y = \tau_*^{-1} + 2\tau_{\text{BR}}^{-1} + 2\tau_{zv,e}^{-1} + 2\tau_{iv,e}^{-1} + 4\tau_{iv,o}^{-1}$	$\tau_{iv,o}^{-1} = \pi\gamma\beta_{x,x}^2/\hbar = \pi\gamma\beta_{x,y}^2/\hbar = \pi\gamma\beta_{y,x}^2/\hbar = \pi\gamma\beta_{y,y}^2/\hbar$
$\Gamma_z^z = 2\tau_{iv}^{-1} + 2\tau_{\text{BR}}^{-1} + 4\tau_{zv,o}^{-1} + 4\tau_{iv,e}^{-1}$	$\gamma = p_F/(2\pi\hbar^2 v)$

and the magnetoresistance, $\Delta\rho(B_z) = \delta\rho(B_z) - \delta\rho(0)$, as

$$\delta\rho(B_z) = -\frac{e^2 \rho^2 D}{\pi\hbar} \sum_{j,l=0,x,y,z} c_j c_l \frac{eB_z}{\pi\hbar} \sum_{n=0}^{\tau_B/\tau} C_j^l(q_n), \quad (8)$$

$$\Delta\rho(B_z) = \frac{e^2 \rho^2}{2\pi\hbar} \sum_{j,l=0,x,y,z} c_j c_l F\left(\frac{B_z}{\mathcal{B}_\varphi + \mathcal{B}_j^l}\right),$$

$$\mathcal{B}_\varphi = \frac{\hbar c}{4De} \tau_\varphi^{-1}, \quad \mathcal{B}_j^l = \frac{\hbar c}{4De} \Gamma_j^l, \quad (9)$$

$$F(z) = \ln z + \psi\left(\frac{1}{2} + \frac{1}{z}\right),$$

where ψ is the digamma function. In Eq. (8), the influence of an external field B_z is taken into account through discrete values $q_n^2 = (n + 1/2)/(D\tau_B)$, where $\tau_B = \hbar/(4DeB_z)$. Used in conjunction with the Cooperon gaps Γ_j^l listed in Table II, Eqs. (6)–(9) provide a general description of the weak-localization correction and corresponding low-field magnetoresistance in the presence of SO coupling in graphene, parametrized by six SO scattering rates τ_{KM}^{-1} , τ_{BR}^{-1} , $\tau_{zv,e}^{-1}$, $\tau_{iv,e}^{-1}$, $\tau_{zv,o}^{-1}$, and $\tau_{iv,o}^{-1}$.

In order to analyze the influence of SO coupling in a realistic experimental situation [13–15], we consider—in the rest of this Letter—the spin-independent intervalley scattering rate τ_{iv}^{-1} to exceed the decoherence rate τ_φ^{-1} and the rates due to SO coupling. This means that $\{\Gamma_j^x, \Gamma_j^y, \Gamma_j^z\} \gg \Gamma_j^0$, and thus the valley-triplet Cooperons in Eqs. (7)–(9) may be neglected. Then, the six SO rates may be combined into just two relevant combinations: a rate τ_{sym}^{-1} due to $z \rightarrow -z$ symmetric SO coupling (the terms \hat{V}_{sym} and \hat{h}_{KM}) and a rate τ_{asy}^{-1} due to $z \rightarrow -z$ asymmetric coupling (\hat{V}_{asy} and \hat{h}_{BR}):

$$\tau_{\text{sym}}^{-1} = \tau_{\text{KM}}^{-1} + 2\tau_{zv,e}^{-1} + 4\tau_{iv,e}^{-1}, \quad (10)$$

$$\tau_{\text{asy}}^{-1} = \tau_{\text{BR}}^{-1} + 2\tau_{zv,o}^{-1} + 4\tau_{iv,o}^{-1}. \quad (11)$$

Here, τ_{BR}^{-1} accounts for the Dyakonov-Perel [23] spin-relaxation contribution, and the other terms account for the Elliott-Yafet [24] spin relaxation.

The application of an in-plane magnetic field produces an interplay between SO coupling and Zeeman splitting, as in semiconductor quantum dots [25,26]. The in-plane magnetic field $\vec{\ell}B_{\parallel}$ introduces an additional term in the Hamiltonian $\delta\hat{H} = (\hbar\omega/2)\vec{\ell}\vec{s}$, where $\omega = 2\mu_B B_{\parallel}/\hbar$, $\epsilon_Z = \hbar\omega$ is the Zeeman energy and $\vec{\ell} = (\ell_x, \ell_y, 0)$, $|\vec{\ell}| = 1$, and we assume that this dominates any orbital effect of the in-plane field [27]. This couples the spin-singlet C_0^0 to the triplets C_x^0 and C_y^0 . The spin part of the matrix equation for the valley singlet Cooperons $(C_0^0, C_x^0, C_y^0, C_z^0) \equiv \mathbf{C}^0$ has the form

$$\begin{pmatrix} \Pi & -i\omega\ell_x & -i\omega\ell_y & 0 \\ -i\omega\ell_x & \Pi + \tau_{\text{so}}^{-1} & 0 & 0 \\ -i\omega\ell_y & 0 & \Pi + \tau_{\text{so}}^{-1} & 0 \\ 0 & 0 & 0 & \Pi + 2\tau_{\text{asy}}^{-1} \end{pmatrix} \mathbf{C}^0 = 1,$$

$$\Pi = D(i\nabla + 2e\mathbf{A}/c\hbar)^2 + \tau_{\varphi}^{-1}, \quad \tau_{\text{so}}^{-1} = \tau_{\text{sym}}^{-1} + \tau_{\text{asy}}^{-1}.$$

After matrix inversion,

$$\begin{aligned} C_0^0 &= \frac{\Pi + \tau_{\text{so}}^{-1}}{\Pi(\Pi + \tau_{\text{so}}^{-1}) + \omega^2} \xrightarrow{\epsilon_Z \rightarrow \infty} 0, \\ C_{x/y}^0 &= \frac{\Pi(\Pi + \tau_{\text{so}}^{-1}) + \omega^2(1 - \ell_{x/y}^2)}{(\Pi + \tau_{\text{so}}^{-1})[\Pi(\Pi + \tau_{\text{so}}^{-1}) + \omega^2]} \xrightarrow{\epsilon_Z \rightarrow \infty} \frac{1 - \ell_{x/y}^2}{\Pi + \tau_{\text{so}}^{-1}}, \\ C_z^0 &= \frac{1}{\Pi + 2\tau_{\text{asy}}^{-1}} \xrightarrow{\epsilon_Z \rightarrow \infty} \frac{1}{\Pi + 2\tau_{\text{asy}}^{-1}}, \end{aligned}$$

where the limit $\epsilon_Z \rightarrow \infty$ of large Zeeman energy essentially means that $\epsilon_Z \gg \hbar\tau_{\text{so}}^{-1}$.

In the absence of an in-plane field, $\epsilon_Z = 0$, the low-field magnetoresistance, Eqs. (8) and (9), is given by

$$\begin{aligned} \Delta\rho &= \frac{e^2\rho^2}{2\pi h} \left[F\left(\frac{B_z}{\mathcal{B}_{\varphi}}\right) - F\left(\frac{B_z}{\mathcal{B}_{\varphi} + \mathcal{B}_{\text{asy}}}\right) - 2F\left(\frac{B_z}{\mathcal{B}_{\varphi} + \mathcal{B}_{\text{so}}}\right) \right], \\ \mathcal{B}_{\text{asy}} &= \frac{\hbar c}{2De}\tau_{\text{asy}}^{-1}, \quad \mathcal{B}_{\text{so}} = \frac{\hbar c}{4De}\tau_{\text{so}}^{-1}. \end{aligned} \quad (12)$$

In the absence of SO coupling, $\mathcal{B}_{\text{so}} = \mathcal{B}_{\text{asy}} = 0$, Eq. (12) would describe negative magnetoresistance corresponding to weak localization [11,12] (lower dashed curves in Fig. 1). In the presence of $z \rightarrow -z$ symmetric SO coupling only, $\mathcal{B}_{\text{asy}} = 0$, the contribution of the third term in Eq. (12) is diminished and the first and second terms cancel each other, leading to a suppression of magnetoresistance for $B_z \lesssim \mathcal{B}_{\text{so}}$ (upper solid curve on the left of Fig. 1) which mimics the effect of a saturated value of τ_{φ}^{-1} : $\tau_{\varphi}^{-1} \rightarrow \tau_{\varphi}^{-1} + \tau_{\text{sym}}^{-1}$. When $z \rightarrow -z$ symmetry is broken, $\mathcal{B}_{\text{asy}} \neq 0$ and $\mathcal{B}_{\text{so}} \neq 0$, there is relaxation of all spin triplets and the second and third terms in Eq. (12) are suppressed, leaving the first (singlet) term to determine antilocalization

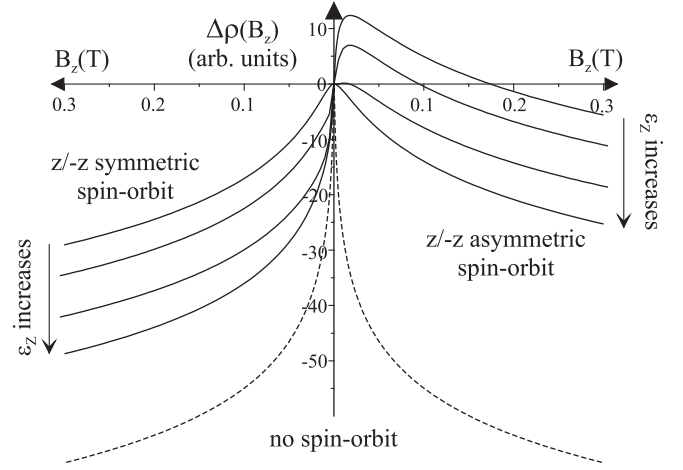


FIG. 1. The low-field magnetoresistivity in the presence of $z \rightarrow -z$ symmetric (left) or asymmetric (right) SO scattering, as compared to the absence of SO scattering (lower dashed curves). Solid curves show the influence of SO scattering, $\tau_{\text{sym}}^{-1} = 25\tau_{\varphi}^{-1}$ and $\tau_{\text{asy}}^{-1} = 25\tau_{\varphi}^{-1}$, respectively, with Zeeman energy $\epsilon_Z = 0$ (top) to $\epsilon_Z \gg \hbar\tau_{\text{so}}^{-1}$ (bottom).

behavior at $T \rightarrow 0$ with positive magnetoresistance at low fields $B_z \lesssim \mathcal{B}_{\text{asy}}$.

In the limit $\epsilon_Z \gg \hbar\tau_{\text{so}}^{-1}$,

$$\Delta\rho = -\frac{e^2\rho^2}{2\pi h} \left[F\left(\frac{B_z}{\mathcal{B}_{\varphi} + \mathcal{B}_{\text{asy}}}\right) + F\left(\frac{B_z}{\mathcal{B}_{\varphi} + \mathcal{B}_{\text{so}}}\right) \right]. \quad (13)$$

This result shows that, for $z \rightarrow -z$ symmetric SO coupling ($\mathcal{B}_{\text{asy}} = 0$), the in-plane field partially restores weak localization at the lowest temperatures, lifting the limitation of τ_{φ} discussed above. In contrast, for $z \rightarrow -z$ asymmetric SO coupling, in-plane field changes weak antilocalization into a suppressed weak-localization behavior. The low-field magnetoresistance calculated using Eq. (8) for intermediate values of ϵ_Z is plotted in Fig. 1, for $z \rightarrow -z$ symmetric (left) and asymmetric (right) SO scattering.

To summarize, among the two extremes of SO coupling in graphene, $z \rightarrow -z$ symmetric and $z \rightarrow -z$ asymmetric, the manifestation of the latter in quantum transport resembles that observed in a 2D electron gas in GaAs/AlGaAs heterostructures, whereas the former is peculiar for graphene. Experimentally, the effect of $z \rightarrow -z$ symmetric SO coupling can be taken for a decoherence time “saturation” [$\tau_{\varphi}(T \rightarrow 0) \rightarrow \tau_{\text{sym}}$] at low temperatures. Unlike inelastic decoherence, such a saturation can be partially lifted by electron Zeeman splitting induced by a strong in-plane magnetic field, making the negative magnetoresistance $\Delta\rho(B_z)$ sharper when $\tau_{\varphi}^{-1}(T \rightarrow 0) \rightarrow 0$. It is necessary to mention that a similar behavior of weak-localization magnetoresistance should be expected in magnetically contaminated conductors [28]. Spin-flip scattering of electrons from localized spins leads to saturation of τ_{φ} at the value of the spin-relaxation time, whereas the

in-plane field freezes local moments, thus suppressing spin-flip scattering of electrons and restoring the full size of the weak-localization effect. However, the size of the in-plane field lifting the saturation of τ_φ in these two cases is different: polarization of magnetic impurities requires $\mu_B B_\parallel > kT$, whereas the suppression of the effect of $z \rightarrow -z$ symmetric SO coupling occurs when $\mu_B B_\parallel > \hbar\tau_{\text{sym}}^{-1}$.

This project has been funded by JST-EPSCRC Japan-UK Cooperative Programme Grant No. EP/H025804/1, EU STREP ConceptGraphene, and the Royal Society.

-
- [1] C.L. Kane and E.J. Mele, *Phys. Rev. Lett.* **95**, 226801 (2005).
- [2] D. Huertas-Hernando, F. Guinea, and A. Brataas, *Phys. Rev. B* **74**, 155426 (2006).
- [3] H. Min, J.E. Hill, N.A. Sinitsyn, B.R. Sahu, L. Kleinman, and A.H. MacDonald, *Phys. Rev. B* **74**, 165310 (2006).
- [4] Y. Yao, F. Ye, X.-L. Qi, S.-C. Zhang, and Z. Fang, *Phys. Rev. B* **75**, 041401 (2007).
- [5] D. Huertas-Hernando, F. Guinea, and A. Brataas, *Phys. Rev. Lett.* **103**, 146801 (2009).
- [6] S. Hikami, A.I. Larkin, and Y. Nagaoka, *Prog. Theor. Phys.* **63**, 707 (1980).
- [7] B.L. Altshuler, D. Khmel'nitzkii, A.I. Larkin, and P.A. Lee, *Phys. Rev. B* **22**, 5142 (1980).
- [8] H. Suzuura and T. Ando, *Phys. Rev. Lett.* **89**, 266603 (2002).
- [9] S.V. Morozov, K.S. Novoselov, M.I. Katsnelson, F. Schedin, L.A. Ponomarenko, D. Jiang, and A.K. Geim, *Phys. Rev. Lett.* **97**, 016801 (2006).
- [10] A.F. Morpurgo and F. Guinea, *Phys. Rev. Lett.* **97**, 196804 (2006).
- [11] E. McCann, K. Kechedzhi, V.I. Fal'ko, H. Suzuura, T. Ando, and B.L. Altshuler, *Phys. Rev. Lett.* **97**, 146805 (2006).
- [12] K. Kechedzhi, E. McCann, V.I. Fal'ko, H. Suzuura, T. Ando, and B.L. Altshuler, *Eur. Phys. J. Special Topics* **148**, 39 (2007).
- [13] F.V. Tikhonenko, D.W. Horsell, R.V. Gorbachev, and A.K. Savchenko, *Phys. Rev. Lett.* **100**, 056802 (2008); F.V. Tikhonenko, A.A. Kozikov, A.K. Savchenko, and R.V. Gorbachev, *ibid.* **103**, 226801 (2009).
- [14] A.A. Kozikov *et al.*, [arXiv:1108.2067v1](https://arxiv.org/abs/1108.2067v1).
- [15] S. Lara-Avila, A. Tzalenchuk, S. Kubatkin, R. Yakimova, T.J.B.M. Janssen, K. Cedergren, T. Bergsten, and V. Fal'ko, *Phys. Rev. Lett.* **107**, 166602 (2011).
- [16] K.-I. Imura, Y. Kuramoto, and K. Nomura, *Phys. Rev. B* **80**, 085119 (2009); *Europhys. Lett.* **89**, 17009 (2010).
- [17] A.H. Castro Neto and F. Guinea, *Phys. Rev. Lett.* **103**, 026804 (2009).
- [18] Y.A. Bychkov and E.I. Rashba, *J. Phys. C* **17**, 6039 (1984).
- [19] E.I. Rashba, *Phys. Rev. B* **79**, 161409 (2009).
- [20] Here, $[s_{j_1}, s_{j_2}] = 2i\varepsilon^{j_1 j_2 j_3} s_{j_3}$, $[\Sigma_{a_1}, \Sigma_{a_2}] = 2i\varepsilon^{a_1 a_2 a_3} \Sigma_{a_3}$, and $[\Lambda_{l_1}, \Lambda_{l_2}] = 2i\varepsilon^{l_1 l_2 l_3} \Lambda_{l_3}$.
- [21] D.M. Basko, *Phys. Rev. B* **78**, 125418 (2008).
- [22] Table I can be used to identify the SO-coupling assisted electron interaction with out-of-plane phonons and static ripples. The degenerate pair of out-of-plane optical (ZO) and out-of-plane acoustic (ZA) phonons at the Brillouin zone corners can be characterized by a four-component vector (u_1, u_2, u_3, u_4) which transforms according to the irreducible representation \tilde{G}' , and this allows the description of the corresponding electron-phonon interaction using $\zeta_1(u_1\Lambda_x s_x + u_2\Lambda_x s_y + u_3\Lambda_y s_x + u_4\Lambda_y s_y)$. The coupling of acoustic ZA phonons and the effect of ripples on the SO coupling can be constructed using the representations \tilde{A}'_1 and \tilde{E}'_2 , and this allows for terms $\zeta_2(\Sigma_x s_y - \Sigma_y s_x)(\partial_x^2 + \partial_y^2)h$ and $\zeta_3[(\Sigma_x s_x - \Sigma_y s_y)(\partial_x^2 - \partial_y^2)h + (\Sigma_x s_y + \Sigma_y s_x)2\partial_x \partial_y h]$ where h is the out-of-plane displacement of the graphene lattice. The constants ζ_1 , ζ_2 , and ζ_3 are linear in the atomic SO coupling.
- [23] M.I. D'yakonov and V.I. Perel, *Sov. Phys. JETP* **33**, 1053 (1971).
- [24] R.J. Elliott, *Phys. Rev.* **96**, 266 (1954); Y. Yafet, in *Solid State Physics*, edited by F. Seitz and D. Turnbull (Academic, New York, 1963), Vol. 14.
- [25] I.L. Aleiner and V.I. Fal'ko, *Phys. Rev. Lett.* **87**, 256801 (2001).
- [26] D.M. Zumbühl, J.B. Miller, C.M. Marcus, K. Campman, and A.C. Gossard, *Phys. Rev. Lett.* **89**, 276803 (2002).
- [27] The Zeeman field, due to the perpendicular magnetic field, suppresses Cooperons C_0^0 and C_z^0 , combining opposite spin components, but this is negligible as compared to the suppression arising from the orbital effect, and thus we ignore it.
- [28] F. Pierre, A.B. Gougam, A. Anthore, H. Pothier, D. Esteve, and N.O. Birge, *Phys. Rev. B* **68**, 085413 (2003).